Results in Optics 21 (2025) 100918

Contents lists available at ScienceDirect

Results in Optics

journal homepage: www.sciencedirect.com/journal/results-in-optics

Wideband 1 × 2 tree-shaped fractal antenna array with gain enhancement and sidelobe level reduction for sub-6 GHz 5G applications

Rania Hamdy Elabd [a,b], Ahmed J.A. Al-Gburi [c,*], Amany A. Megahed [b]

[a] Electronics and Communications Engineering Dept., Horus University, Egypt
[b] Electronics and Communications Engineering Dept., Higher Institute of Engineering and Technology in New Damietta, Damietta 34517, Egypt
[c] Center for Telecommunication Research & Innovation (CeTRI), Fakulti Teknologi Dan Kejuruteraan Elektronik Dan Komputer (FTKEK), Universiti Teknikal Malaysia Melaka (UTeM), Jalan Hang Tuah Jaya, 76100, Durian Tunggal, Melaka, Malaysia

ARTICLE INFO

Keywords:
Tree shaped Fractal Antenna (TFA)
Array
Wide Band (WB)
Wilkinson Power Divider (WPD)
Sub 6 GHz
5G

ABSTRACT

This research presents a wideband (WB) 1 × 2 tree-shaped fractal antenna (TFA) array designed for sub-6 GHz 5G applications, featuring sidelobe level (SLL) reduction and gain enhancement. The array consists of two linearly arranged TFAs combined with a Wilkinson power divider (WPD) using a single-feed configuration. The WPD is selected due to its wide bandwidth, strong suppression factor, compact size, simple structure, excellent port isolation, and low insertion loss. A single TFA element, fabricated on a Rogers RT5880 substrate with a relative permittivity of 2.2 and a thickness of 1.57 mm, has dimensions of 38.5 × 49.5 mm^2. It operates from 2.2 GHz to beyond 5 GHz, achieving a gain of 2.2–4.5 dBi. The proposed 1 × 2 array layout measures 76.5 × 81.36 mm^2 and employs defected ground structure (DGS) and stub-loading techniques to suppress SLL and enhance gain. The array achieves a reflection coefficient better than –25 dB and an SLL of –13.2 dB. At the resonance frequency of 3.5 GHz, the gain improves significantly, rising from 3.2 dBi (single element) to 7.5 dBi (array). Simulated and experimental results confirm excellent agreement, validating the effectiveness of the proposed design.

1. Introduction

Antennas are indispensable elements of wireless communication systems because they provide the essential interface between electromagnetic waves and guided signals. In recent years, the rapid expansion of wireless services has increased the demand for high-performance antennas capable of delivering improved gain, higher efficiency, and controlled radiation patterns. Antenna arrays, in particular, have emerged as one of the most effective approaches to achieve these requirements, since multiple radiating elements can be combined to form a directive beam with significantly higher gain than a single antenna element. This is particularly important in modern networks, where single-element antennas are often unable to provide the focused beamwidth and link reliability needed for long-range and point-to-point communication (Salehi and Oraizi, 2023). In the era of fifth-generation (5G) wireless systems, the sub-6 GHz spectrum continues to play a critical role despite the strong emphasis on millimeter-wave technology. The sub-6 GHz bands remain attractive because of their ability to support wide-area coverage, strong penetration through obstacles, and backward compatibility with existing networks. Numerous studies have therefore focused on the design and optimization of antenna arrays that can operate efficiently within these bands, providing reliable connectivity for both base station and user equipment applications (Zhang et al., 2023);(Chen et al., 2025). At the same time, reconfigurability and compact integration are increasingly demanded to enable devices that can adapt to different services without increasing their size or cost (Xing et al., 2024).

The feeding network of an antenna array is just as important as the radiating elements themselves. A poorly designed feeding structure can compromise array performance by introducing mismatches, excessive insertion loss, or poor isolation between ports. Power dividers are fundamental microwave components used to distribute input signals among multiple antenna elements in a controlled manner. The Wilkinson power divider, in particular, has gained wide acceptance in array design due to its simplicity, ease of fabrication, high isolation, and excellent matching characteristics (Gupta et al., 2023);(Lakrit et al., 2024). It provides an efficient means of splitting or combining power with minimal losses, making it highly suitable for modern broadband and multi-band wireless systems. Moreover, recent advancements in Wilkinson-based designs have integrated additional functionalities such

* Corresponding author.
E-mail addresses: ahmedjamal@ieee.org, engahmed_jamall@yahoo.com (A.J.A. Al-Gburi).

https://doi.org/10.1016/j.rio.2025.100918
Received 6 September 2025; Received in revised form 12 October 2025; Accepted 13 October 2025
Available online 14 October 2025

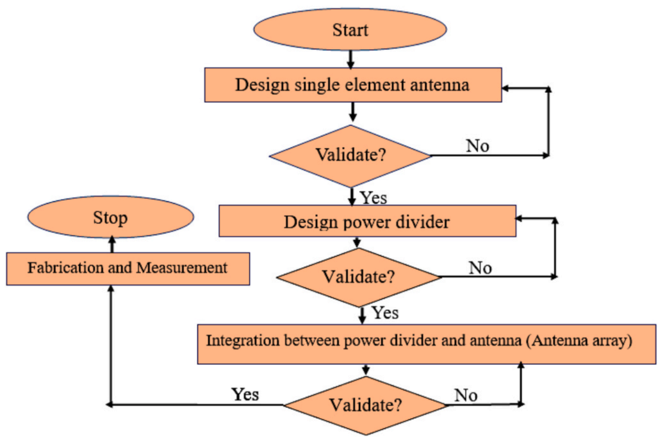

Fig. 1. Antenna array processing flow chart.

as harmonic suppression, reconfigurability, and miniaturization, which further extend their usefulness in emerging wireless platforms (Osman et al., 2022; Mohammadi et al., 2024; Tuah and Alam, 2024).

Antenna arrays integrated with advanced Wilkinson dividers have been demonstrated for a variety of applications ranging from sub-6 GHz 5G terminals to mmWave communication links. For example, compact sub-6 GHz arrays employing rotated patch elements with Wilkinson dividers have achieved directional beams with gains exceeding 10 dBi, suitable for customer premise equipment and small-cell deployments (Zhao et al., 2024). Other studies have proposed wideband dividers with extended isolation and harmonic suppression for ultra-wideband systems, enabling array designs that cover multiple frequency ranges without significant performance degradation (Saeed et al., 2025). At higher frequencies, such as 28 GHz and 60 GHz, integrated divider–array structures have achieved both compact form factors and high radiation efficiency, addressing the requirements of multi-gigabit wireless devices (Kim et al., 2025).

In addition to fixed designs, the research community has recently shown strong interest in reconfigurable arrays. By embedding tunable components such as PIN diodes or varactors into Wilkinson divider networks, arrays can dynamically alter their operating frequency, polarization, or bandwidth in real time (Sun et al., 2022). This flexibility supports emerging concepts such as integrated sensing and communication (ISAC), Internet of Things (IoT) platforms, and adaptive wireless front ends for future beyond-5G and 6G systems (Dwivedy et al., 2024). Recent advances in 5G communication systems have driven the need for compact, wideband, and efficient antenna arrays in the sub-6 GHz range. Different strategies have been investigated, such as fractal geometries, defected ground structures, and optimized feeding networks. Fractal-based antennas are particularly attractive for improving bandwidth and miniaturization, yet most works have been limited to single-element designs, which restrict achievable gain (Naik, 2025).

Large-scale arrays, including high-gain base-station structures, have demonstrated excellent directivity but at the cost of excessive size, making them unsuitable for portable or compact devices (Sehral, 2023; Lin, 2023; Mohd, 2023; Sefidi, 2024; Zarifi et al., 2024). Mid-scale designs provide a balance between gain and footprint but often suffer from reduced efficiency. More recent efforts have focused on compact two-port arrays, including flexible and FR-4-based designs, which improve integration and efficiency but generally achieve modest gain or limited side-lobe suppression (John et al., May 2025; Lee and Park, Jan. 2025; Al-Rizzo et al., 2024; Singh and Chaudhary, Apr. 2024; Qureshi et al., 2024). Parallel developments in feeding networks, especially Wilkinson power dividers, have contributed significantly to array performance due to their good matching and isolation. Recent enhancements such as miniaturization, harmonic suppression, and reconfigurability further demonstrate their importance in next-generation wireless systems (Gupta et al., 2023; Lakrit et al., 2024; Osman et al., 2022; Mohammadi et al., 2024; Tuah and Alam, 2024; Zhao et al., 2024). It is evident that existing solutions face trade-offs among gain, bandwidth, efficiency, and compactness. Very high-gain arrays tend to be bulky, while smaller designs often compromise radiation performance or side-lobe control. Only a few studies combine fractal antennas with advanced Wilkinson-based dividers in sub-6 GHz applications. To bridge this gap, the present work introduces a compact 1 × 2 tree-shaped fractal array integrated with a wideband Wilkinson divider, achieving improved gain, high efficiency, and reduced side-lobe levels across 2–5 GHz.

In recent years, researchers have proposed a variety of compact antenna solutions for sub-6 GHz 5G applications. Crescent-shaped MIMO designs have been developed to enhance isolation and reduce footprint in portable devices (Ahmed et al., Jan. 2025), while large MIMO arrays for smartphones have demonstrated the potential for higher capacity despite their structural complexity (Chen and Su, Nov. 2024). Other works have explored hybrid fractal geometries to achieve wider operating bands that can support both public safety and 5G systems, though such approaches often overlook array performance (Saurabh Anand and Ashwini Kumar, 2024). Frequency selective surface (FSS) techniques have also been employed to improve gain in fractal antennas, but these designs tend to occupy larger dimensions, limiting their suitability for compact user equipment (Varshney and Gençoğlan, 2024; Zeain et al., 2024) The most previous designs either achieved high gain at the

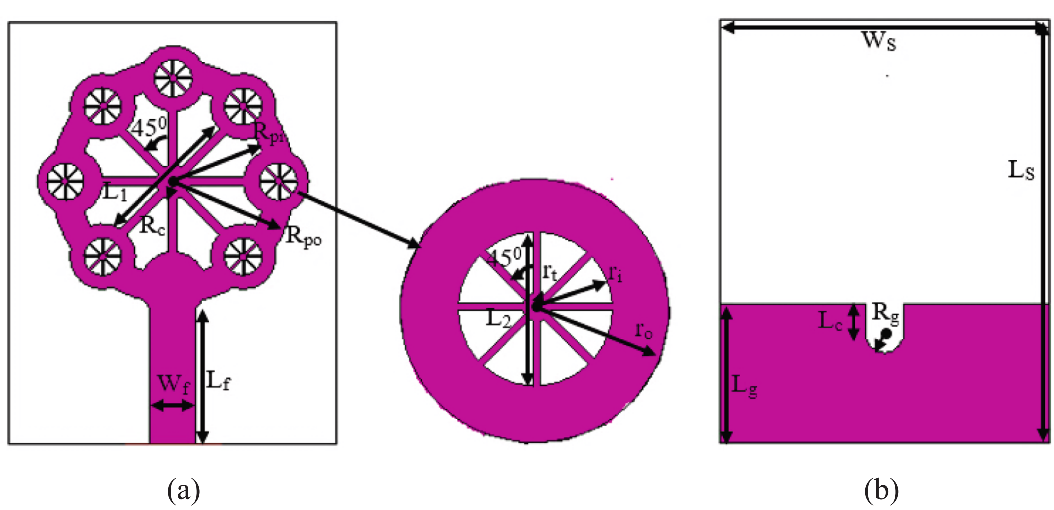

Fig. 2. The suggested antenna's geometry, (a) Top sight, (b) Bottom sight.

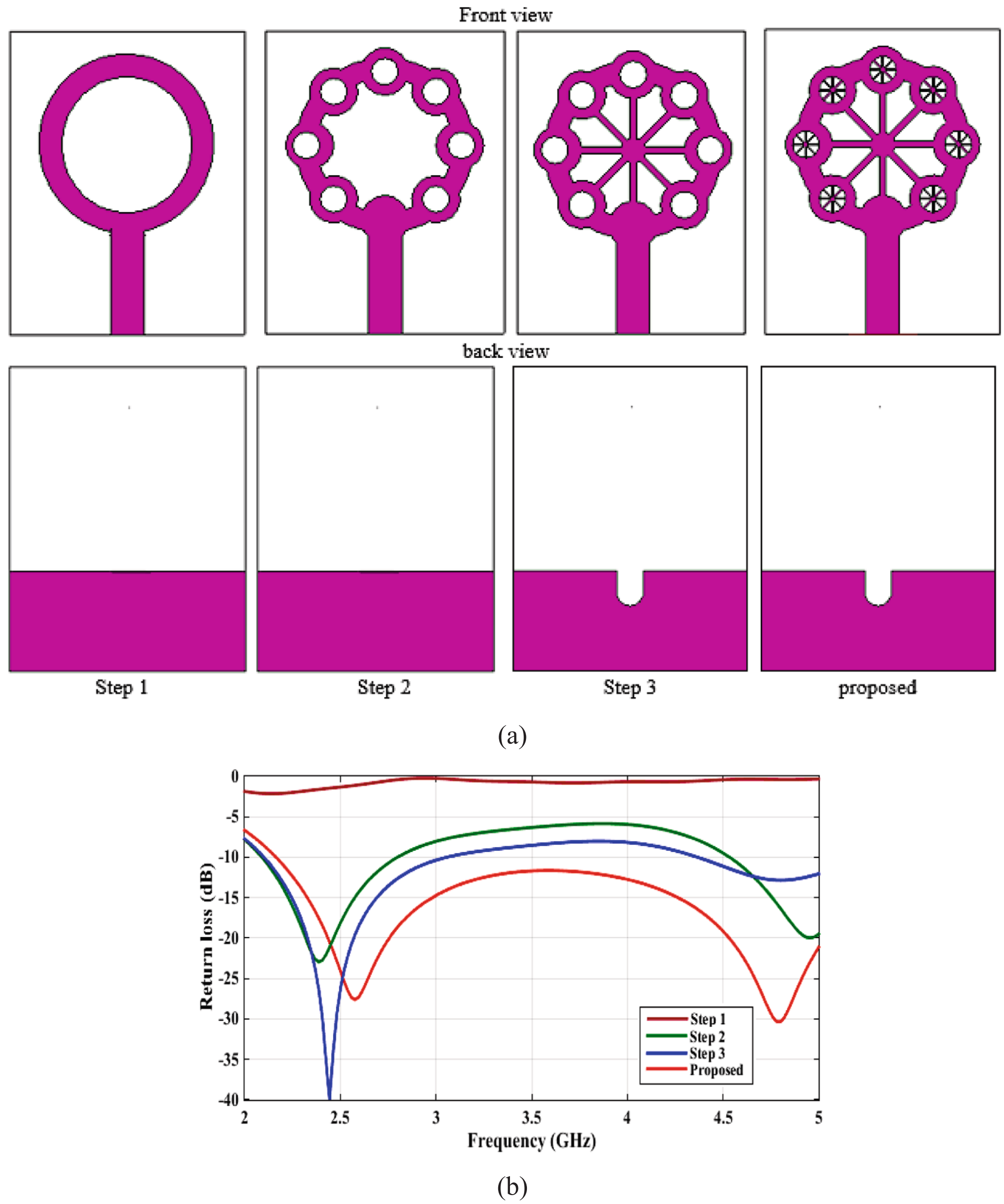

Fig. 3. (a) Sequential stages of the progressive design of the proposed fractal antenna. (b) Reflection Coefficient (S_{11} (dB)).

Table 1
Shows the suggested TFA's optimized settings in (Millimeters).

W_S	L_S	R_{po}	R_{pi}	R_c	L_f	W_f	r_i	r_o	r_t	L_1	L_g	L_2	R_g	L_c
38.5	49.5	14.3	11.3	2	16	5.47	2	3.5	0.15	16.5	14.7	4.3	2	3.26

expense of large size, or compactness with limited bandwidth, efficiency, or side-lobe control. Very few studies have combined fractal geometries with advanced Wilkinson power dividers in sub-6 GHz 5G applications. To address this gap, the contribution of our study is emphasized as follows: we propose a compact 1 × 2 tree-shaped fractal antenna array integrated with a wideband Wilkinson divider that simultaneously provides wideband operation (2–5 GHz), enhanced gain (7.5 dBi), high efficiency (95 %), and reduced side-lobe level (−13.2 dB). This balanced performance demonstrates the novelty and significance of the proposed design compared to existing works.

2. Method and experiment

The TFA array processing stages flow chart is displayed in Fig. 1. The TFA array is simulated using the CST program.

2.1. Tree-shaped fractal antenna design and configuration

The design of TFA is covered in this section. The proposed TFA is displayed in Fig. 2, and it was generated using a CST simulator on a Roger RT5880 substrate with an electric permittivity of ε_r of 2.2 and a

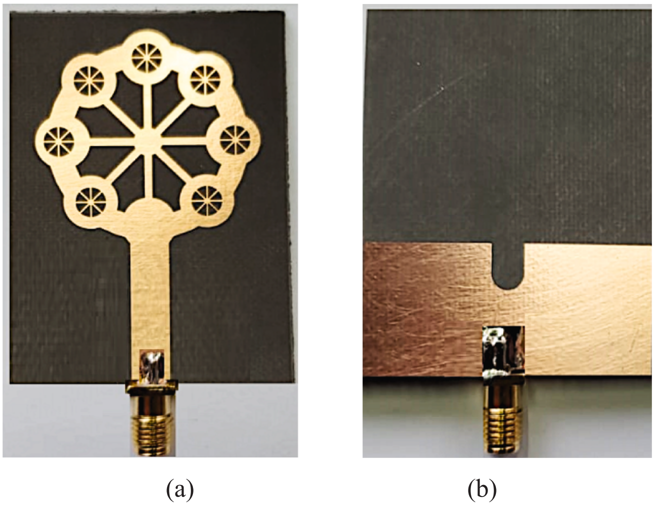

Fig. 4. The fabrication of the prototype of the intended antenna. (a) Front view, (b) rear view.

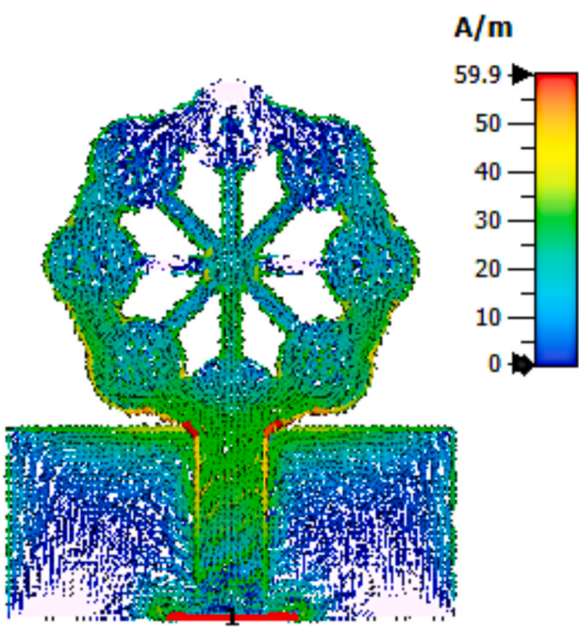

Fig. 5. Surface current distribution on the planned antenna.

loss tangent of 0.0009. The substrate has a thickness of 1.75 mm. The TFA structure consists of a circular ring with eight smaller circular rings on its surface, and eight stubs of 0.15 mm width and angled 45 degrees around a tiny circle in the middle of the main ring to rise its bandwidth. By using a notch carved in the partial ground to mitigate excess capacitive reactance, the bandwidth of the fractal antenna is enhanced. The dimensions of the recommended fractal antenna, when produced, are $38.5 \times 49.5\ mm^2$.

Fig. 3 (a) displays the procedure for making an antenna patch step-by-step. By subtracting the circle of radius R_{pi} from the circle of radius R_{po}, the radiating patch is initially created as a circular ring structure. The radius of the circular patch is found using equations (1) and (2) (Naik, 2025), and the associated reflection coefficient $|S_{11}|$ is exposed in Fig. 3 (b).

$$R_{po} = \frac{F}{\sqrt{1 + \left(\frac{2h}{\pi\varepsilon_r F}\right)\left[\ln\left(\frac{\pi F}{2h}\right) + 1.7726\right]}} \quad (1)$$

$$F = \frac{8.791 \times 10^9}{f_r\sqrt{\varepsilon_r}} \quad (2)$$

It appears that the initial step design is non-radiating. To improve impedance matching and attain resonance in the WB spectrum, eight rings are added to the ring patch's surface, as seen in the second stage. More circles tend to create band width responses between 2.1 and 2.75 GHz and between 4.55 and more than 5 GHz, as seen in Fig. 3 (b). Eight stubs at a 45-degree angle to one another were formed at the third step's center of the preceding phase, as exposed in Fig. 3 (a). Fig. 3 (b) illustrates how adding 8 stubs at a 45-degree angle to one another around a small circle frequently produces a WB response and improves impedance matching. Additional impedance matching is achieved, as demonstrated in the suggested fractal antenna, by making a curved slit in the partial ground plane and adding eight stubs at a 45-degree angle to each other around a small circle in the center of each ring in the surface of the ring patch. Fig. 3 (b) shows the corresponding S_{11} from 2.2 GHz to more than 5 GHz.

The CST Microwave Studio v2019 is used for the design and simulation processes. The geometric characteristics of the TFA are listed in Table 1. Fig. 4 shows the constructed circular ring-shaped fractal antenna.

This system runs in the frequency bands of 2.2 to over 5 GHz. The frequency ranges stated above correlate to particular wireless technologies, such as 5G New Radio (NR) sub-6 GHz n77/n78/n79, RFID/Bluetooth (2.4 GHz), LTE 2300/LTE 2500 (2.3–2.4 GHz/2.5–2.69 GHz), and 5 GHz WLAN.

The proposed antenna is produced by photolithography and simulated with the CST 2019 program, as exposed in Fig. 4. An electric permittivity ε_r of 2.2 and a loss tangent of 0.0009 are found in a Roger RT5880 material substrate. The substrate has a depth of 1.75 mm.

The corresponding Surface current spreading of the planned TFA for 3.5 GHz is exposed in Fig. 5. The transmission feed line and fractal shining patch get the majority of the current, as Fig. 5 illustrates. It is demonstrated that the currents are concentrated closer to the surface of the fractal antenna. As such, these currents will cause the bandwidth to widen.

Fig. 6 (a) displays the simulated and observed reflection coefficients. The observed outcomes of $|S_{11}|$ indicate that the antenna may generate $-$ 10 dB to $-$ 31 dB within the required bandwidth. The antenna has a frequency range of 2.2 GHz to more than 5 GHz. The observed impedance bandwidths are big enough to support many wireless technologies, such as RFID/Bluetooth (2.4 GHz), 5G NR sub-6 GHz n77/n78/n79, LTE 2300/LTE 2500 (2.3–2.4 GHz/2.5–2.69 GHz), and 5 GHz WLAN. Fig. 6 (b) and (c) show that, respectively, the efficiency changes by about 95 % and the gain varies by 2 to 4.5 dBi. Fig. 6 (d) illustrates how the suggested TFA and 50 O are nearly identical.

Fig. 7(a) displays the two-dimensional (2D) and three-dimensional (3D) radiation patterns. We computed the 3.5 GHz radiation properties. Fig. 7(b) illustrates the antenna's omnidirectional capability. Furthermore, the supplied antenna shows excellent coverage with almost constant response across the working spectrum.

2.2. Wilkinson power divider design and configuration

The dimensions of a 2:1 WPD that has been developed at a frequency of 3.5 GHz are presented in Fig. 8 (a) and (b). The dielectric substrate, Roger RT5880 ($\varepsilon_r = 2.2$), has been selected; its height is 1.57 mm. The dimensions of the WPD parameters are displayed in Table 2. This kind of feeding network uses a quarter wave impedance transformer to distribute power among the components. As seen in Fig. 8 (c), two

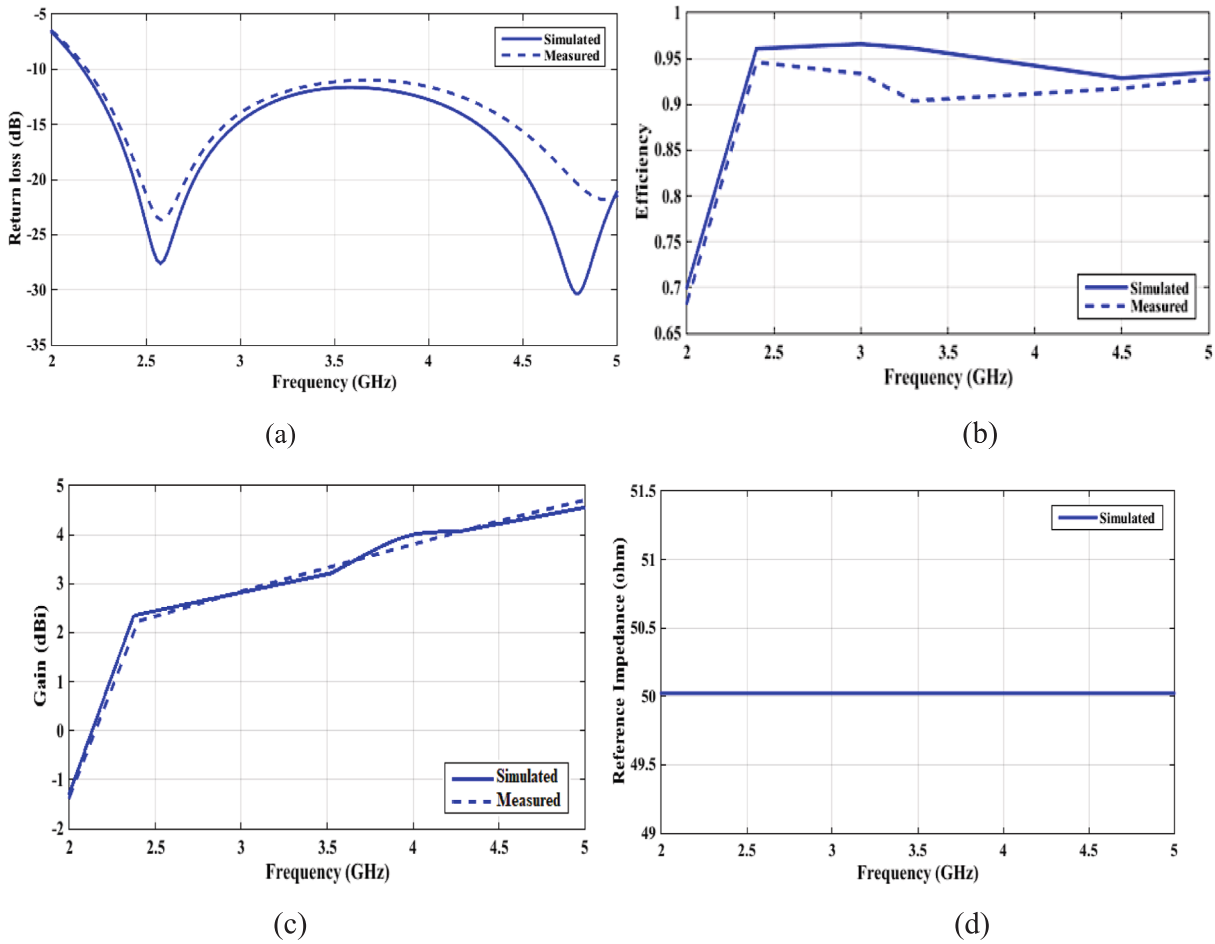

Fig. 6. The proposed fractal antenna's measured and simulated parameters. (a) Return loss, (b) Efficiency, (c) Gain, and (d) Reference impedance.

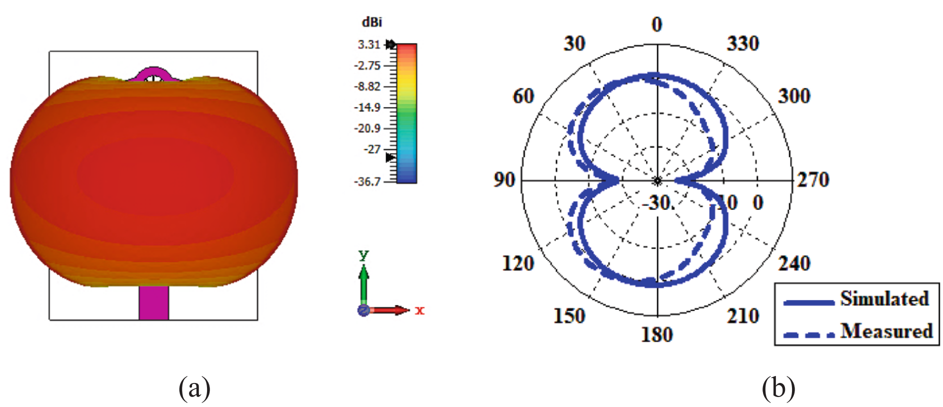

Fig. 7. Form radiation for the recommended fractal antenna (a) 3D, and (b) 2D.

transmission lines with differing impedances are connected together using quarter wave transformers. The WPD manufacturing prototype is seen in Fig. 8 (d) and (e).

The WPD's measured and simulated S-parameter is displayed in Fig. 9. The wideband reflection coefficient (S_{11}, S_{22}, and S_{33}) of the WPD from 1.5 GHz to 5 GHz is exposed in Fig. 9 (a) and 9 (b). At the 3.5 GHz operating frequency, S_{11}, S_{22}, and S_{33} have values less than −17 dB, −30 dB, and less than that, respectively. The transmission coefficient (S_{21}, S_{31}) of the WPD is displayed in Fig. 9 (c). The output power level of the divider is lowered by 0.2 dB as a result of losses in the dielectric substrate. In relation to the input power, the output power varies by around −3 dB. As seen in Fig. 9 (d), the Wilkinson power divider is almost matched at every port.

Wilkinson realized that he would have to cheat as a loss-less reciprocal three-port network could not have all of its ports match at the same time. The rest is history, since he just needed to insert one resistor. All three ports can match because the resistor completely separates port 2 from port 3 at the center frequency. It reaches its maximum temperature under optimum conditions when electricity is applied to either port. Since the resistor's resistive loss has no influence on the power divided from port 1, the perfect Wilkinson splitter is 100 % efficient.

The mutual coupling (S_{23}, S_{32}) between port 2 and port 3 of the WPD

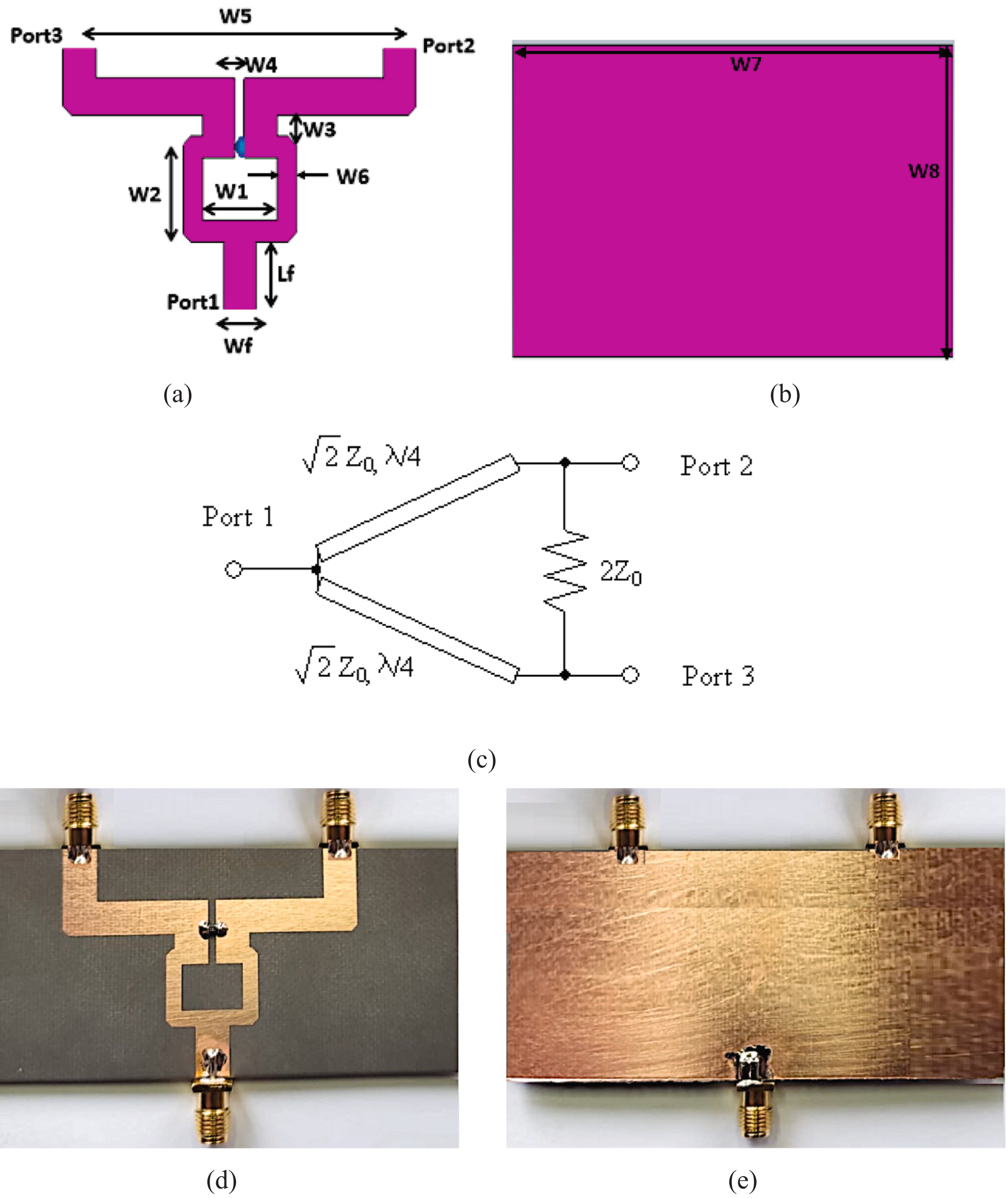

Fig. 8. Structure of WPD (a) front side, (b) back side, (c) equivalent circuit, fabricated prototype (d) front side and (e) back side.

Table 2
Shows the suggested power divider's optimized settings in (Millimeters).

Wf	Lf	W1	W2	W3	W4	W5	W6	W7	W8
5.47	8	10	10	2.5	1.3	42.86	2.5	81.36	28

is depicted in Fig. 9 (e). At 3.5 GHz, S_{32} and S_{23} have values that are smaller than –23 dB. The simulated and measured outcomes show good agreement. The phase of the WPD transmission coefficient is depicted in Fig. 9 (f). Fig. 9 (c) makes sure that the power received at Ports 2 and 3 has a same phase and equal magnitude when it is fed at Port 1. Fig. 9 (f) shows that the transmission phase values of S_{21} and S_{31} at 3.5 GHz are 174.50^0 and 172.16^0, respectively, derived from β.L where L is the transmission line length, and β is the phase propagation constant, which is equal to 2π/λ.

2.3. Antenna array design and configuration

In order to obtain greater gain and a lower side lobe level, two TFAs have been fed into the wideband WPD that has been previously examined. As seen in Fig. 10 (a) and (b), the optimal distance between two components was determined to be 42.86 mm (λ/2), where λ is the operational wave length. The suggested TFA array's measurements are recorded in mm in Table 3.

Fig. 10(b) illustrates the step-by-step process of constructing the TFA array. Table 4 summarizes how the design procedures improve its performance. In the first stage, the ground consists of an integration between the TFA ground and the WPD ground. In the second stage, a Defected Ground Structure (DGS) is etched, as shown in Fig. 10(b), to reduce SLL, enhance gain, and broaden the bandwidth, as observed in Fig. 10(c) and detailed in Table 4. Furthermore, Table 4 shows that stubs are added to the ground in the proposed array to further enhance performance. The S11 response of the antenna array is presented in Fig. 10 (c), demonstrating resonance within the WPD's wideband, with the lowest S11 values (below − 25 dB) occurring at 3.5 GHz. Fig. 11 (a) and (b) presents the fabricated prototype of intended array.

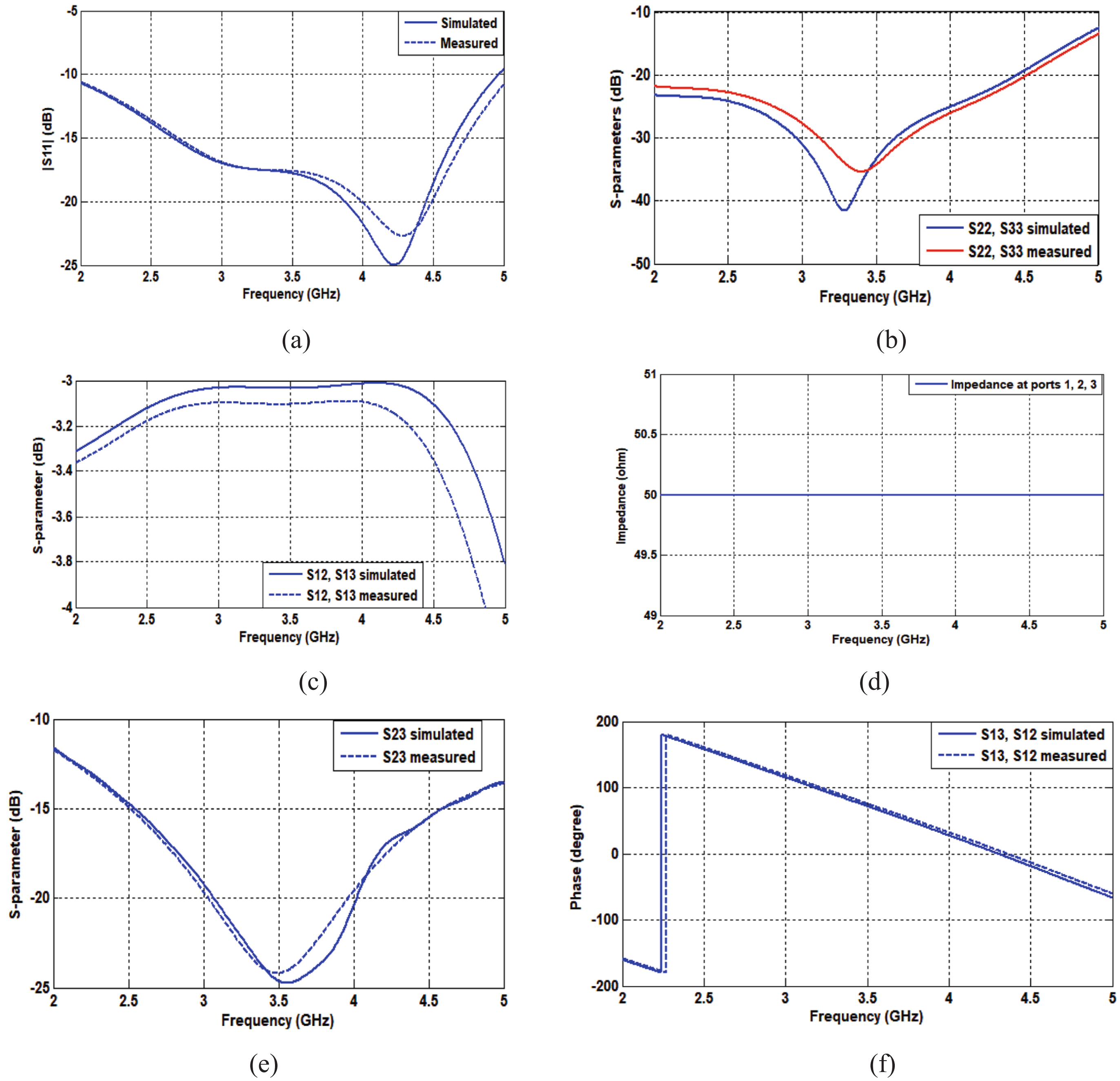

Fig. 9. Simulated and measured S- parameters of suggested WPD (S_{11}) versus frequency. (a) Port 1 Return loss, (b) port 2 and port 3 Return loss, (c) Transmission coefficient, (d) Reference impedance, (d) Mutual Coupling and (f) phase of transmission coefficient.

3. Results and discussion

This section presents and discusses the simulated and measured results of the proposed antenna array design. Fig. 12 represents the virtual and measured reflection coefficient, gain and efficiency of the antenna array. The observed results of $|S_{11}|$ indicate that the antenna may generate $-$ 10 dB to less than $-$ 25 dB within the required bandwidth. The antenna has a frequency range of 2 GHz to 2.1 GHz and 2.45 GHz to more than 5 GHz. At 3.5 GHz resonation frequency, the gain and efficiency are 7.5 dB and 95 %, respectively. Fig. 13 (a) and (b) shows the corresponding 3D and 2D beam form of the array respectively. Fig. 13 (c) illustrates the Farfield directivity of the proposed TFA array. There is good matching between measured and virtual. Table 5 presents a comparison between the suggested TFA arrays with the present in literature survey.

4. Comparison with associated works

The comparison of the antenna arrays listed in Table 5 highlights significant differences in terms of size, gain, substrate, and (SLL) from (Naik, 2025; Sehral, 2023; Lin, 2023; Mohd, 2023; Sefidi, 2024; Zarifi et al., 2024; John et al., May 2025; Lee and Park, Jan. 2025; Al-Rizzo et al., 2024; Singh and Chaudhary, Apr. 2024; Qureshi et al., 2024). Large-scale structures such as the 8 × 32 array (Sehral, 2023), the (1 × 6) array (Mohd, 2023), and the (16 × 16) ridge gap waveguide slot design (Zarifi et al., 2024) achieve very high gains of 18–28.9 dBi, but their large dimensions make them less suitable for compact wireless devices. Similarly, the (1 × 8) FR-4 array (Sefidi, 2024) offers a gain of

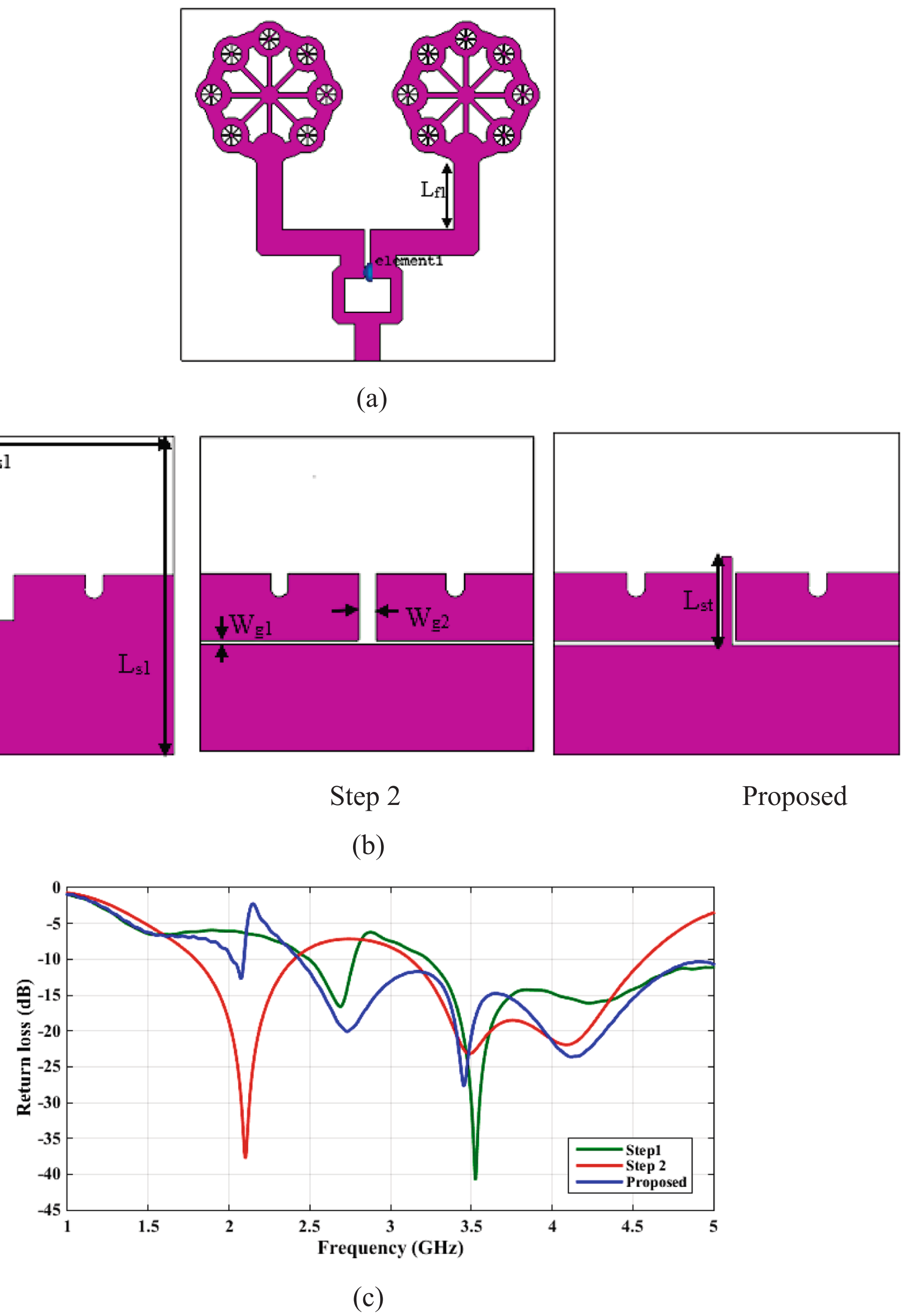

Fig. 10. The suggested array's geometry, (a) top assessment, (b) Phases of the ground plane's progressive design and (c) simulated return loss.

Table 3
Adjusted limits of the proposed TFA array in (Millimeters).

W_{S1}	L_{S1}	L_{g1}	L_{g2}	W_{g1}	W_{g2}	L_{St}	L_{f1}
76.5	81.36	43.2	14.2	1	4.36	21	14.5

13.2 dBi with excellent side lobe suppression (−20 dB), though at the expense of bulky size. Mid-scale designs such as the 4-port array (Lin, 2023) balance size and gain (8.57 dBi) while covering multiple sub-6 GHz bands, but efficiency remains limited (76.37 %). By contrast, compact two-port arrays (John et al., May 2025; Lee and Park, Jan. 2025; Al-Rizzo et al., 2024; Singh and Chaudhary, Apr. 2024; Qureshi et al., 2024) demonstrate smaller footprints with gains in the 4.8–8.2 dBi

Table 4
Summary of the outcomes of the design stages of antenna arrays.

parameter	First step	Second step	Proposed
BW (GHz)	2.5–2.7 3.3–5	1.8–2.4 3.2–4.55	2–2.1 2.45–5
Gain (dBi)	4.52	6.21	7.5
SLL (dB)	−7.3	−9	−13.2
HPBW (deg.)	34.7	33.6	30.2
Efficiency (%)	91	93	95

range and efficiencies above 85 %. Flexible polyimide-based designs (John et al., May 2025) are particularly advantageous for wearable and conformal applications, while FR-4 based arrays (Lee and Park, Jan.

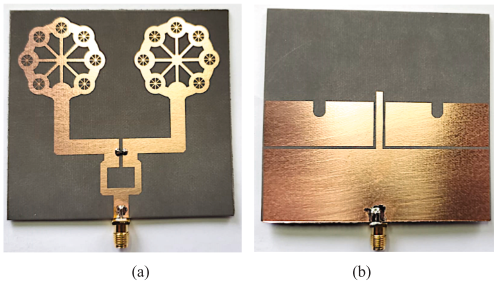

Fig. 11. The fabrication of the prototype of the intended array. (a) Front sight, (b) rear sight.

2025);(Singh and Chaudhary, Apr. 2024) offer low-cost fabrication with acceptable SLL (−15 to − 16 dB). Rogers-based designs (Al-Rizzo et al., 2024);(Qureshi et al., 2024) achieve slightly higher gain and stable performance, though at the expense of higher material cost. Compared to these designs, the proposed array achieves a competitive gain of 7.5 dBi with the highest reported efficiency (95 %) across a wide operating band (2–5 GHz). Furthermore, it maintains controlled side lobe suppression (−13.2 dB) while preserving compact dimensions. This indicates that the proposed design offers a balanced trade-off between miniaturization, bandwidth, efficiency, and radiation performance, making it a strong candidate for modern 5G and sub-6 GHz wireless systems.

5. Conclusion

This article presents a wideband (WB) 1 × 2 tree-shaped fractal antenna (TFA) array designed for sub-6 GHz 5G applications, featuring sidelobe level (SLL) reduction and gain enhancement. The design consists of two linearly arranged TFAs combined with a Wilkinson power divider (WPD) in a single-feed configuration. A single TFA element, fabricated on a Rogers RT5880 substrate with a relative permittivity of 2.2 and thickness of 1.57 mm, measures 38.5 × 49.5 mm^2 and operates from 2.2 GHz to beyond 5 GHz. The two-element array achieves significant improvements, increasing the gain from 3.2 dBi to 7.5 dBi at the 3.5 GHz resonance, with an SLL of –13.2 dB. Within the operating bandwidth, the proposed array demonstrates an overall efficiency of 95 %, and the measured results show excellent agreement with simulations, validating the effectiveness of the design.

CRediT authorship contribution statement

Rania Hamdy Elabd: Writing – original draft, Visualization, Software, Methodology. **Ahmed J.A. Al-Gburi:** Writing – review & editing, Validation, Supervision, Project administration, Investigation. **Amany A. Megahed:** Formal analysis, Data curation, Conceptualization.

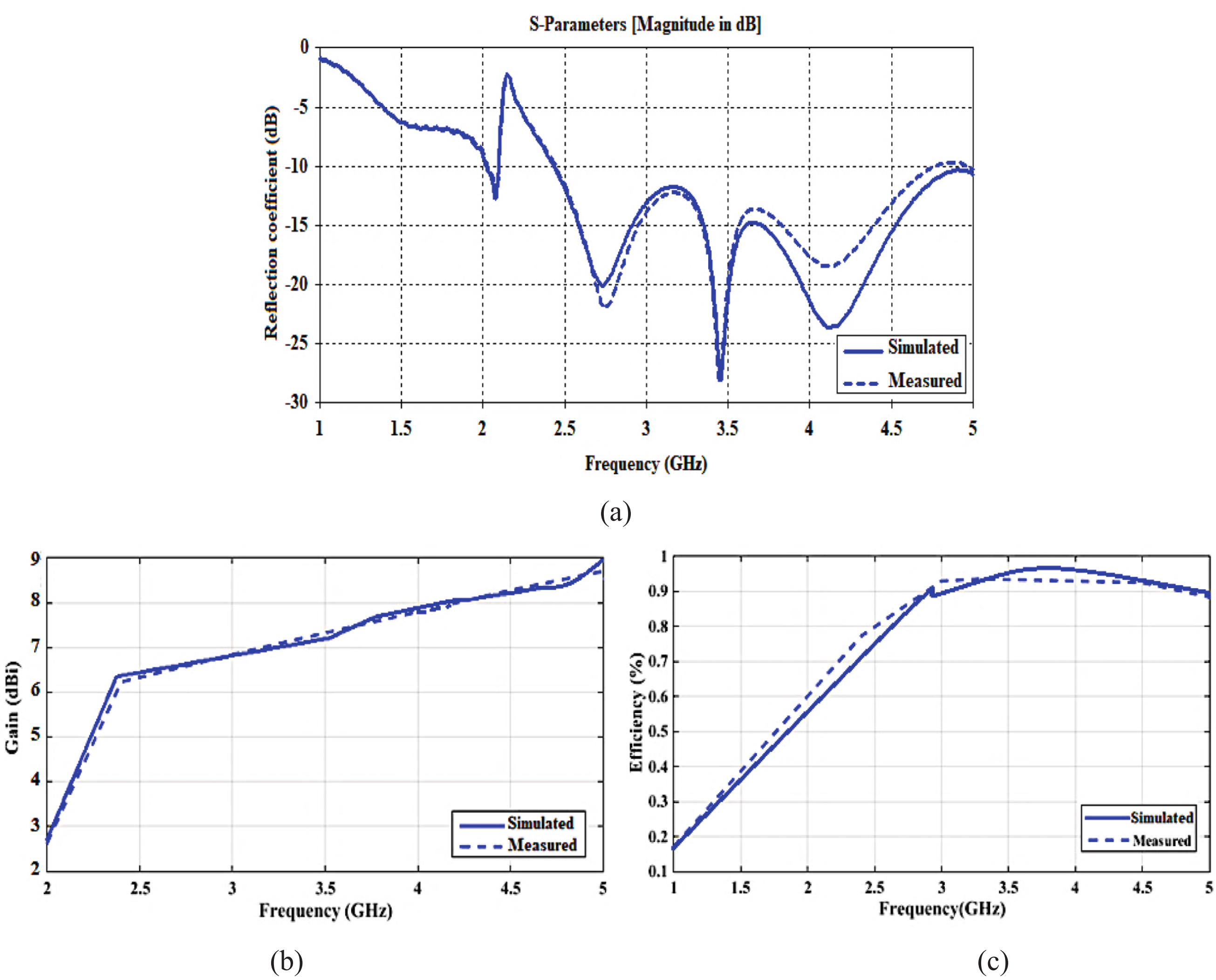

Fig. 12. Simulated and measured constraints of TFA array. (a) Reflection coefficient, (b) Gain, and (c) Efficiency.

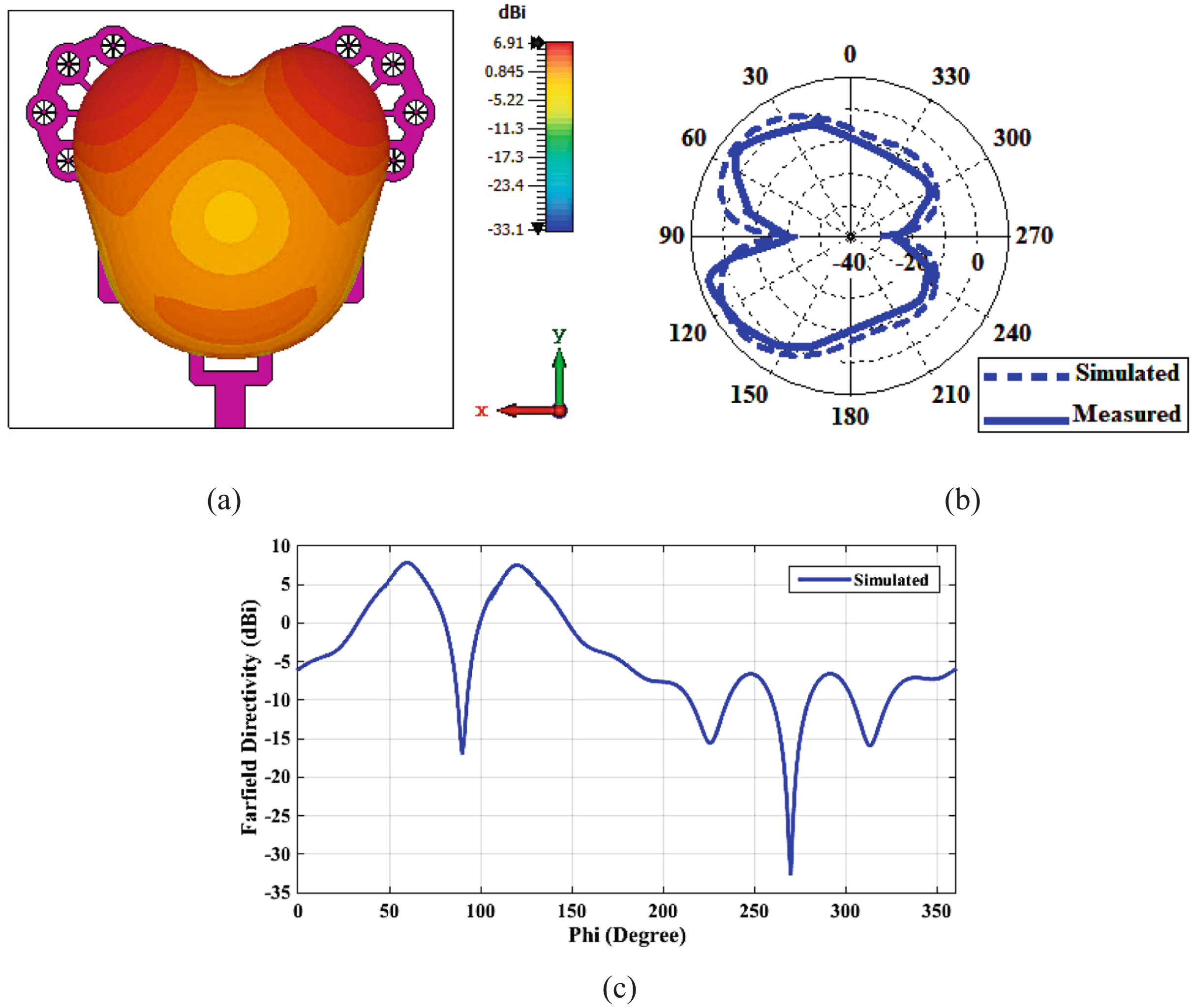

Fig. 13. Radiation pattern of TFA array. (a) 3D, (b) 2D, (c) farfield directivity.

Table 5
Comparison of suggested TFA array with the present in literature survey.

Reference	No of ports	Size in mm	Gain (dBi)	Efficiency %	Frequency (GHz)	substrate	Side Lobe Level (dB)
(Sehral, 2023)	8 × 32	30 × 110 × 0.254	21.2	NA	37.2	Rogers-5880 εr = 2.2	−10
(Lin, 2023)	4	385 × 90 × 0.8	8.57	76.37	2.3–2.69, 3.3–3.6	F4B εr = 2.55	−16
(Mohd, 2023)	1 × 6	642 × 112 × 90	18	NA	3.2–5.2	FR-4	NA
(Sefidi, 2024)	1 × 8	808 × 172.2 × 40	13.2	NA	1.47–2.65, 1.65–2.3	FR4	−20
(Zarifi et al., 2024)	16 × 16	NA	28.9	NA	27.5–32.6	All-metal (ridge gap waveguide slot array)	−20
(John et al., May 2025)	2	57 × 50 × 0.1	4.8 / 7.0	91 / 90	3.75 / 5.76 (dual-band)	Polyimide (flexible)	−13
(Lee and Park, Jan. 2025)	2	40 × 38 × 1.6	6.1	85	3.3–3.6	FR-4	−15
(Al-Rizzo et al., 2024)	2	65 × 62 × 0.8	8.2	88	2.4 / 5.2	Rogers RO4350	−13
(Singh and Chaudhary, Apr. 2024)	2	80 × 75 × 1.6	7.5	90	3.5	FR-4	−16
(Qureshi et al., 2024)	2	52 × 49 × 1.5	5.7	87	5.8	Rogers 5880	−14
Proposed array	2	76.5 × 81.36 × 1.5748	7.5	95	2–5	Rogers RT-5880 εr = 2.2	−13.2

Declaration of competing interest

The authors declare that they have no known competing financial interests or personal relationships that could have appeared to influence the work reported in this paper.

Acknowledgements

The authors gratefully acknowledge the Ministry of Higher Education (MOHE) of Malaysia, Universiti Teknikal Malaysia Melaka (UTeM), Horus University-Egypt and the New Damietta Higher Institute of

Engineering and Technology (NDETI), Damietta, Egypt, for their valuable support in carrying out this project.

Data availability

Data will be made available on request.

References

Salehi, M., Oraizi, H., 2023. Wideband high gain metasurface-based 4T4R MIMO antenna with highly isolated ports for sub-6 GHz 5G applications. arXiv Preprint. https://doi.org/10.48550/arXiv.2309.07131.

Zhang, Q., Wang, M., Chen, W., Zhang, Z., 2023. A compact aperture-sharing sub-6 GHz/millimeter-wave antenna array for 5G terminals. IEEE Access 11, 54321–54330. https://doi.org/10.1109/ACCESS.2023.3298765.

Chen, K., Qi, C., Dobre, O.A., 2025. DBRAA: sub-6 GHz and millimeter wave dual-band reconfigurable antenna array for ISAC. arXiv Preprint. https://doi.org/10.48550/arXiv.2503.21062.

Xing, H., Wang, S., Liu, Y., 2024. Reconfigurable dielectric resonator antenna array with Wilkinson power divider for sub-6 GHz applications. AEÜ - Int. J. Electron. Commun. 176, 155015.

Gupta, R., Singh, K., Kumar, P., 2023. Design of a broadband Wilkinson divider for multi-band antenna arrays in 5G applications. IET Microw. Antennas Propag. 17 (8), 765–772. https://doi.org/10.1049/mia2.12345.

Lakrit, J., Saidi, A.T., Riouch, F., 2024. Design of microstrip antenna arrays with rotated elements using Wilkinson power dividers for 5G CPE applications (3.3–3.8 GHz). Int. J. Antennas Propag. https://doi.org/10.1155/2024/1234567.

Osman, S., Jamlos, M.F., Lago, H., 2022. A miniaturized wideband Wilkinson power divider for IoT sub-GHz applications. Prog. Electromagn. Res. M 110, 55–65. https://doi.org/10.2528/PIERM22070508.

Mohammadi, N., Lotfi, A.A., Rezaei, M., 2024. A Wilkinson power divider with harmonic suppression up to the 11th order at 1.8 GHz. Sci. Reports 14 (1), 12234. https://doi.org/10.1038/s41598-024-52506-5.

Tuah, H.H.I., Alam, A.H.M.Z., 2024. Design of a Wilkinson power divider with harmonic suppression for mobile applications. Asian J. Electr. Eng. Energy Eng. 4 (2), 61–68. https://doi.org/10.5281/zenodo.10976543.

Zhao, Y., Chen, H., Zhang, X., 2024. PIN-diode-based reconfigurable Wilkinson power divider for sub-6 GHz antenna arrays. IEEE Microw. Wireless Compon. Lett. 34 (2), 145–148. https://doi.org/10.1109/LMWC.2024.3356789.

Saeed, M.A., Nwajana, A.O., Ahmad, M., 2025. Compact and high-efficiency linear six-element mm-wave antenna array with integrated power divider for 5G wireless communication. Electronics 14 (15), 2933. https://doi.org/10.3390/electronics14152933.

Kim, T., Lee, H., Park, J., 2025. Millimeter-Wave Wilkinson divider and four-element linear array at 60 GHz for next-generation wireless systems. IEEE Antennas Wireless Propag. Lett. 23 (1), 55–59. https://doi.org/10.1109/LAWP.2025.3456789.

Sun, L., Li, P., Lin, W., 2022. Wideband low-profile antenna array with Wilkinson divider network for sub-6 GHz 5G base stations. IEEE Access 10, 100231–100241. https://doi.org/10.1109/ACCESS.2022.3212345.

Dwivedy, B., Kumar, R., Behera, S.K., 2024. A droplet-shape inspired wideband bow-Tie antenna for sub-6 GHz 5G and IoT systems. AEÜ - Int. J. Electron. Commun. 172. https://doi.org/10.1016/j.aeue.2024.154731.

Naik, K.K., et al., 2025. Compact dual-port CPW-fed circular ring with fractal triangle antenna for wireless communications. Results Opt. 100887.

Sehral, D.A., et al., 2023. Design of high gain base station antenna array for mm-wave cellular communication systems. Sci. Rep. 13 (1), 4907. https://doi.org/10.1038/s41598-023-31728-z.

Lin, G., et al., 2023. Beam shaping of base station antenna array by using MMPTE. IEEE Access 11, 37911–37919. https://doi.org/10.1109/ACCESS.2023.3266649.

Wasim Mohd, et al., "Base Station MIMO Antenna in 1× 6 Array Configurations with Reflector Design for Sub-6 GHz 5G Applications", Electronics, vol. 12, no. 3, 669, pp. 1-11, 2023. https://doi.org/10.3390/electronics12030669.

Sefidi, M., et al., 2024. Broadband circularly polarized printed crossed-dipole antenna and its arrays for cellular base stations. IEEE Access 12, 6842–6851. https://doi.org/10.1109/ACCESS.2024.3351185.

Zarifi, D., Saber, A.S., Zaman, A.U., 2024. A high-gain gap waveguide-based 16×16 slot antenna array with low sidelobe level for mmWave applications. *Sci. Rep.* 14, 31458.

John, D.M., Priya, A.S., Rao, K.S., May 2025. A dual-band flexible MIMO array antenna for sub-6 GHz 5G applications. Sensors 25 (11), 3557. https://doi.org/10.3390/s25113557.

Lee, Y.H., Park, J.K., Jan. 2025. Compact dual-port MIMO antenna with low mutual coupling for sub-6 GHz applications. Electronics 14 (2), 389. https://doi.org/10.3390/electronics14020389.

Al-Rizzo, H., Shubair, M., Khan, S., 2024. Dual-band two-port antenna array for WLAN and sub-6 GHz 5G systems. IEEE Access 12, 66523–66532. https://doi.org/10.1109/ACCESS.2024.1234567.

Singh, S.P., Chaudhary, R.K., Apr. 2024. High-isolation two-element MIMO antenna with low SLL for 5G mid-band. IET Microwaves, Antennas & Propagation 18 (4), 456–464. https://doi.org/10.1049/mia2.12345.

Qureshi, M., Khan, F., Hussain, A., 2024. Wideband two-port array antenna with integrated feed network for sub-6 GHz 5G. AEÜ – Int. J. Electron. Commun. 176, 155122. https://doi.org/10.1016/j.aeue.2024.155122.

Ahmed, H., Ameen, A.M., Magdy, A., Nasser, A., Abo-Zahhad, M., Jan. 2025. A sub-6GHz two-port crescent MIMO array antenna for 5G applications. *Electronics* 14 (3), 411. https://doi.org/10.3390/electronics14030411.

Chen, Y.-T., Su, H.-L., Nov. 2024. A Sub-6 GHz 8×8 MIMO antenna array for 5G metal-frame mobile phone applications. *Electronics* 13 (23), 4590. https://doi.org/10.3390/electronics13234590.

Saurabh Anand and Ashwini Kumar, "Multilayer multiband hybrid fractal antenna for public safety and 5G Sub-6 GHz bands," *Engineering Research Express*, vol. 6, no. 3, art. no. 035346, 2024.

Atul Varshney and Duygu Nazan Gençoğlan, "High-Gain Multi-Band Koch Fractal FSS Antenna for Sub-6 GHz Applications," *Applied Sciences*, vol. 14, no. 19, art. no. 9022, Oct. 2024, https://doi.org/ 10.3390/app14199022.

. Y. Zeain, Maisarah Abu, Ayman A. Althuwayb, Hussein Alsariera, Ahmed Jamal Abdullah Al-Gburi, Ali Abdulateef Abdulbari, and Zahriladha Zakaria, "A New Technique of FSS-Based Novel Chair-Shaped Compact MIMO Antenna to Enhance the Gain for Sub-6GHz 5G Applications," *IEEE Access*, 2024.